The Astrophysical Journal Supplement Series, 207:39 (8pp), 2013 August doi:10.1088/0067-0049/207/2/39

THE INTERPLANETARY NETWORK SUPPLEMENT TO THE *FERMI* GBM CATALOG OF COSMIC GAMMA-RAY BURSTS

K. Hurley[1], V. D. Pal'shin[2], R. L. Aptekar[2], S. V. Golenetskii[2], D. D. Frederiks[2], E. P. Mazets[2,21], D. S. Svinkin[2], M. S. Briggs[3], V. Connaughton[3], C. Meegan[4], J. Goldsten[5], W. Boynton[6], C. Fellows[6], K. Harshman[6], I. G. Mitrofanov[7], D. V. Golovin[7], A. S. Kozyrev[7], M. L. Litvak[7], A. B. Sanin[7], A. Rau[8], A. von Kienlin[8], X. Zhang[8], K. Yamaoka[9], Y. Fukazawa[10], Y. Hanabata[10], M. Ohno[10], T. Takahashi[11], M. Tashiro[12], Y. Terada[12], T. Murakami[13], K. Makishima[14,22], S. Barthelmy[15], T. Cline[15,23], N. Gehrels[15], J. Cummings[16,24], H. A. Krimm[17,25], D. M. Smith[18], E. Del Monte[19], M. Feroci[19], and M. Marisaldi[20]

[1] University of California, Berkeley, Space Sciences Laboratory, 7 Gauss Way, Berkeley, CA 94720-7450, USA; khurley@ssl.berkeley.edu
[2] Ioffe Physical Technical Institute, St. Petersburg 194021, Russia
[3] University of Alabama in Huntsville, NSSTC, 320 Sparkman Drive, Huntsville, AL 35805, USA
[4] Universities Space Research Association, NSSTC, 320 Sparkman Drive, Huntsville, AL 35805, USA
[5] Applied Physics Laboratory, Johns Hopkins University, Laurel, MD 20723, USA
[6] University of Arizona, Department of Planetary Sciences, Tucson, AZ 85721, USA
[7] Space Research Institute, 84/32, Profsoyuznaya, Moscow 117997, Russia
[8] Max-Planck-Institut für extraterrestrische Physik, Giessenbachstrasse, Postfach 1312, D-85748 Garching, Germany
[9] Division of Particle and Astrophysical Science, Graduate School of Science, Nagoya University, Furo-cho, Chikusa-ku, Nagoya 464-8602, Japan
[10] Department of Physics, Hiroshima University, 1-3-1 Kagamiyama, Higashi-Hiroshima, Hiroshima 739-8526, Japan
[11] Institute of Space and Astronautical Science (ISAS/JAXA), 3-1-1 Yoshinodai, Sagamihara, Kanagawa 229-8510, Japan
[12] Department of Physics, Saitama University, 255 Shimo-Okubo, Sakura-ku, Saitama-shi, Saitama 338-8570, Japan
[13] Department of Physics, Kanazawa University, Kadoma-cho, Kanazawa, Ishikawa 920-1192, Japan
[14] Department of Physics, University of Tokyo, 7-3-1 Hongo, Bunkyo-ku, Tokyo 113-0033, Japan
[15] NASA Goddard Space Flight Center, Code 661, Greenbelt, MD 20771, USA
[16] UMBC/CRESST/NASA Goddard Space Flight Center, Code 661, Greenbelt, MD 20771, USA
[17] CRESST/NASA Goddard Space Flight Center, Code 661, Greenbelt, MD 20771, USA
[18] Physics Department and Santa Cruz Institute for Particle Physics, University of California, Santa Cruz, Santa Cruz, CA 95064, USA
[19] INAF/IASF-Roma, via Fosso del Cavaliere 100, I-00133 Roma, Italy
[20] INAF/IASF-Bologna, Via Gobetti 101, I-40129 Bologna, Italy
Received 2013 April 11; accepted 2013 June 21; published 2013 August 2

ABSTRACT

We present Interplanetary Network (IPN) data for the gamma-ray bursts in the first *Fermi* Gamma-Ray Burst Monitor (GBM) catalog. Of the 491 bursts in that catalog, covering 2008 July 12 to 2010 July 11, 427 were observed by at least one other instrument in the nine-spacecraft IPN. Of the 427, the localizations of 149 could be improved by arrival time analysis (or "triangulation"). For any given burst observed by the GBM and one other distant spacecraft, triangulation gives an annulus of possible arrival directions whose half-width varies between about 0.′4 and 32°, depending on the intensity, time history, and arrival direction of the burst, as well as the distance between the spacecraft. We find that the IPN localizations intersect the 1σ GBM error circles in only 52% of the cases, if no systematic uncertainty is assumed for the latter. If a 6° systematic uncertainty is assumed and added in quadrature, the two localization samples agree about 87% of the time, as would be expected. If we then multiply the resulting error radii by a factor of three, the two samples agree in slightly over 98% of the cases, providing a good estimate of the GBM 3σ error radius. The IPN 3σ error boxes have areas between about 1 arcmin^2 and 110 deg^2, and are, on the average, a factor of 180 smaller than the corresponding GBM localizations. We identify two bursts in the IPN/GBM sample that did not appear in the GBM catalog. In one case, the GBM triggered on a terrestrial gamma flash, and in the other, its origin was given as "uncertain." We also discuss the sensitivity and calibration of the IPN.

Key words: catalogs – gamma-ray burst: general – techniques: miscellaneous

Online-only material: color figure, figure set, machine-readable tables

1. INTRODUCTION

This paper presents the latest in a series of catalogs of gamma-ray burst (GRB) localizations obtained by arrival time analysis, or "triangulation" between the spacecraft in the third Interplanetary Network (IPN; Table 1). In the present paper, we present the localization data on 149 bursts which occurred during the period covered by the first, two-year *Fermi* Gamma-Ray Burst Monitor (GBM) GRB catalog (Paciesas et al. 2012; 2008 July 12 to 2010 July 11). As the composition of the IPN has changed over the years, we present a summary of the instrumentation and techniques in the following section. Section 3 contains the localization data, which are also available on the IPN Web site.[26] In Section 4, we discuss the statistics of the localizations.

[21] Deceased.
[22] Makishima Cosmic Radiation Laboratory, The Institute of Physical and Chemical Research (RIKEN), 2-1 Hirosawa, Wako, Saitama 351-0198, Japan.
[23] Emeritus.
[24] Joint Center for Astrophysics, University of Maryland, Baltimore County, 1000 Hilltop Circle, Baltimore, MD 21250.
[25] Universities Space Research Association, 10211 Wincopin Circle, Suite 500, Columbia, MD 21044.

[26] http://ssl.berkeley.edu/ipn3/index.html

Table 1
Recent IPN Catalogs of Gamma-Ray Bursts

Years Covered	Number of GRBs	Description
1990–1992	16	*Ulysses, Pioneer Venus Orbiter,* WATCH, SIGMA, PHEBUS GRBs[a]
1990–1994	56	*Granat*-WATCH supplement[b]
1991–1992	37	*Pioneer Venus Orbiter, Compton Gamma-Ray Observatory, Ulysses* GRBs[c]
1991–1994	218	BATSE 3B supplement[d]
1991–2000	211	BATSE untriggered burst supplement[e]
1992–1993	9	*Mars Observer* GRBs[f]
1994–1996	147	BATSE 4Br supplement[g]
1994–2012	271	Konus short bursts[h]
1996–2000	343	BATSE 5B supplement[i]
1996–2002	475	*BeppoSAX* supplement[j]
2000–2006	226	HETE-2 supplement[k]
2008–2010	146	GBM supplement[l]

Notes.
[a] Hurley et al. (2000b); [b] Hurley et al. (2000c); [c] Laros et al. (1998); [d] Hurley et al. (1999a); [e] Hurley et al. (2005); [f] Laros et al. (1997); [g] Hurley et al. (1999b); [h] Pal'shin et al. (2013); [i] Hurley et al. (2011b); [j] Hurley et al. (2010); [k] Hurley et al. (2011a); [l] Present catalog.

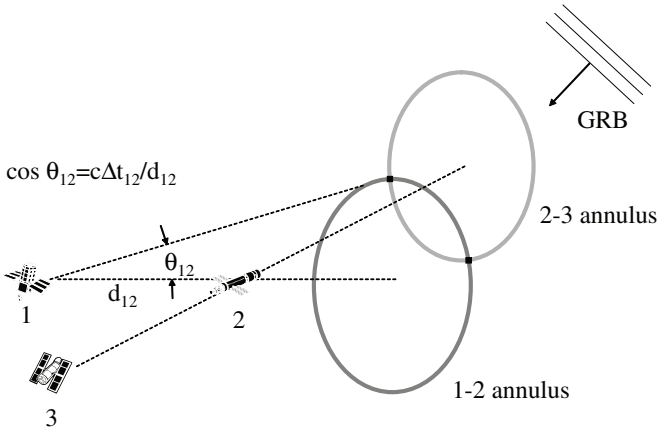

Figure 1. The triangulation technique. Each independent spacecraft pair is used to derive an annulus of location for the burst. Three spacecraft produce two possible error boxes. The ambiguity can be eliminated by the addition of a fourth, non-coplanar spacecraft by the anisotropic response of one of the experiments, or by the GBM localization.

2. TECHNIQUE, INSTRUMENTATION, CALIBRATION, AND SENSITIVITY

The triangulation technique is illustrated in Figure 1. When a GRB arrives at two spacecraft with a delay δT, it may be localized to an annulus whose half-angle θ with respect to the vector joining the two spacecraft is given by

$$\cos\theta = \frac{c\delta T}{D} \quad (1)$$

where c is the speed of light and D is the distance between the two spacecraft. (This assumes that the burst is a plane wave, i.e., that its distance is much greater than D.) The annulus width $d\theta$, and thus one dimension of the resulting error box, is

$$d\theta = c\sigma(\delta T)/D\sin\theta \quad (2)$$

where $\sigma(\delta T)$ is the uncertainty in the time delay. The radius of each annulus and the right ascension and declination of its center are calculated in a heliocentric (i.e., aberration-corrected) frame.

The composition of the missions and experiments comprising the interplanetary network changes as old missions are terminated and new missions are introduced. During the period covered in the present catalog, the IPN consisted of *Konus-Wind*, at distances up to around 5 lt-s from Earth (Aptekar et al. 1995); *Mars Odyssey*, in orbit around Mars at up to 1250 lt-s from Earth (Hurley et al. 2006); the *International Gamma-Ray Laboratory* (*INTEGRAL*), in an eccentric Earth orbit at up to 0.5 lt-s from Earth (Rau et al. 2005); the *Mercury Surface, Space Environment, Geochemistry, and Ranging* mission (*MESSENGER*), launched in 2004 August, and in an eccentric orbit around Mercury beginning 2011 March 18, up to 690 lt-s from Earth (Gold et al. 2001); and the *Ramaty High Energy Solar Spectroscopic Imager* (*RHESSI*; Smith et al. 2002), *Swift* (Goldstein et al. 2012), *Fermi* (Meegan et al. 2009), *Suzaku* (Takahashi et al. 2007; Yamaoka et al. 2009), and *AGILE* (Marisaldi et al. 2008; Del Monte et al. 2008; Tavani et al. 2009), all in low Earth orbit.

The detectors in the IPN vary widely in shape, composition, time resolution, and energy range. Also, onboard timekeeping techniques and accuracies are not the same from mission to mission, and spacecraft ephemeris data are given only as predicts for some missions. Since the accuracy of the triangulation technique depends on all these parameters, end-to-end calibrations and sensitivity checks are a constant necessity. For the current IPN, we utilize the following method. For every burst for which the *Swift* X-Ray Telescope (XRT) detects an X-ray afterglow, we search for GRB detections in all the IPN experiments. If the burst was detected by (1) *Odyssey* and *Konus* or by *Odyssey* and a near-Earth mission, (2) *MESSENGER* and *Konus* or by *MESSENGER* and a near-Earth mission, or (3) *Konus* and a near-Earth mission, we derive an IPN annulus by triangulation. We then calculate the angle between the annulus center line and the XRT position θ_X, taken from the GCN Circulars, and which we take to be a point source, because its positional uncertainty is much less than the annulus width $d\theta$ (Figure 2). $d\theta$ is calculated such that the distribution of annulus widths is approximately Gaussian, so the distribution of $\theta_X/d\theta$ should follow a normal distribution with mean zero and standard deviation 1, if systematic uncertainties are neglected. We have used this procedure so far for 78 *MESSENGER*/*Konus* or *MESSENGER*/near-Earth triangulations, 292 *Konus*/near-Earth triangulations, and 72 *Odyssey*/*Konus* or *Odyssey*/near-Earth triangulations. We find that for the interplanetary spacecraft a systematic uncertainty equal to roughly 0.75 times the statistical one is required to make the

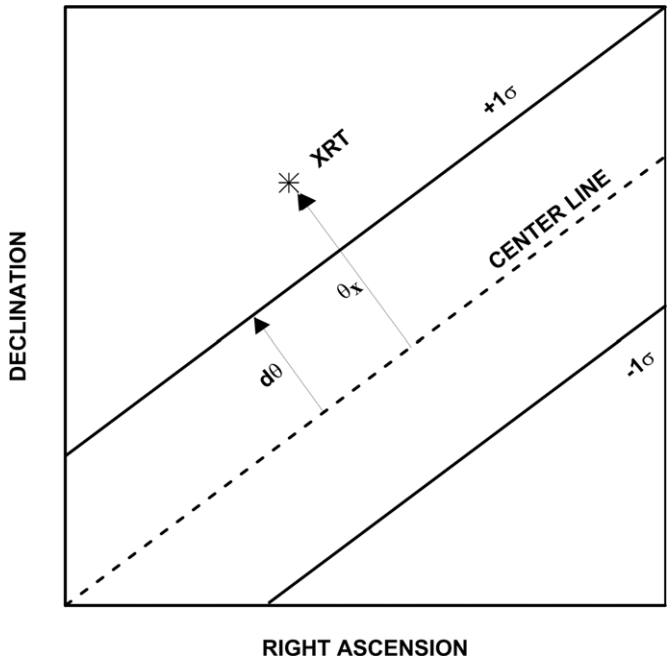

Figure 2. Closeup of a portion of a triangulation annulus. The dashed line is the center line, and the two solid lines are the 1σ contours. The 1σ annulus width is $d\theta$, and the minimum angle between the center line and the XRT counterpart is θ_X.

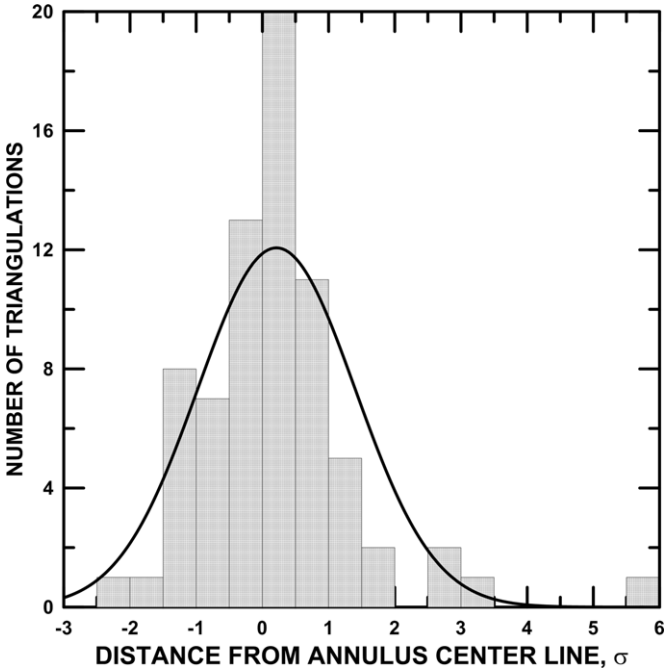

Figure 3. *MESSENGER* triangulation accuracy. The histogram shows the angles between the annuli center lines and the XRT counterparts for 78 bursts. The mean is 0.11 and the standard deviation is 0.96. A systematic uncertainty equal to 0.75 times the statistical uncertainty has been assumed. The solid line is a Gaussian fit to the histogram.

distributions consistent with normal distributions. An example is shown in Figure 3. Systematic uncertainties arise from numerous sources. Some are certainly negligible in some cases, while others may be important. But in almost all cases, it is impossible to assign an accurate number to them. A partial list follows, in no particular order.

1. Variations in the clock accuracy from one spacecraft to another. Different spacecraft have different ways of calibrating their clocks and assigning times to the time bins of GRB time histories. We know, for example, that in some cases the GRB timing is subject to uncertainties, even though the spacecraft oscillator is quite accurate.
2. Predict timing. In many cases, the time assigned to a GRB is a predicted time, and it is never updated. In other cases, such as *Odyssey* and *MESSENGER*, the time is eventually updated using an accurate model for the clock drift; in this study, the updated times have been used for these spacecraft. In other cases, no final clock corrections are applied.
3. Different time resolutions. For any given spacecraft pair, the time resolutions can be vastly different, and sometimes one is not an exact multiple of the other. One time history is adjusted to match the time resolution of the other spacecraft in the light curve comparisons. This can be done in a variety of ways, but each is subject to uncertainties. Even in cases where one time resolution is in principle an exact multiple of another, the true values of the bin widths can be slightly different from their nominal values due to different on-board electronics.
4. Spacecraft ephemerides. Some ephemerides are predictions, while others are final. In these comparisons, the final ephemerides were used where possible, but they were not always available.
5. Different energy responses of the various detectors. In most cases, the GRB light curves are recorded in different energy ranges from one another. Even in those cases where we attempt to match the energy ranges of the detectors (i.e., where the photons are energy-tagged), the detector responses within those ranges are different due to the very different detector designs.

It is often possible to derive very precise triangulation annuli for bursts detected by *Konus* and the GBM, even though the distance between the spacecraft is not large. The reasons are first, that the first 1.024 s of triggered *Konus* data are transmitted with 2 ms time resolution; this is the finest resolution of all the IPN detectors which bin their data. Second, GBM time- and energy-tagged data can be utilized to match Konus' time bins and energy range, minimizing two possible sources of systematic uncertainties. Thus for short-duration or intense GRBs, or bursts with fine time structure, *Konus*/GBM annulus widths as small as several arcminutes can be obtained (Pal'shin et al. 2013). To verify Konus-GBM triangulations we have derived Konus-GBM triangulation annuli for 52 precisely localized bursts. The 3σ half-widths of these annuli range from $0\overset{\circ}{.}11$ to $21\overset{\circ}{.}8$ with a mean of $3\overset{\circ}{.}0$ and a geometrical mean of $1\overset{\circ}{.}19$. Figure 4 shows the distribution of the offsets (in sigma) of the precise positions. The mean offset is 0.09 and the standard deviation is 0.77. The minimum offset is −1.40 and the maximum is 1.69.

To calibrate the IPN sensitivity, we use estimates of the peak fluxes, fluences, durations, and $E_{\rm peak}$ of a large number of GBM bursts.[27] These are measured in the 50–300 keV range, and are given in photons $\rm cm^{-2}\ s^{-1}$ (measured over a 1024 ms period), erg $\rm cm^{-2}$, s, and keV, respectively. At the time this catalog was submitted in its final version, there were 1078 GBM bursts with peak flux, fluence, and duration entries, and 482 with $E_{\rm peak}$ entries. To calculate the IPN sensitivity, we determined (1) whether any other IPN spacecraft also detected the burst, and (2) whether *Konus*, *MESSENGER*, or *Odyssey* detected the burst. Only the latter detections can lead to meaningful

[27] http://heasarc.gsfc.nasa.gov/cgi-bin/W3Browse/w3query.pl

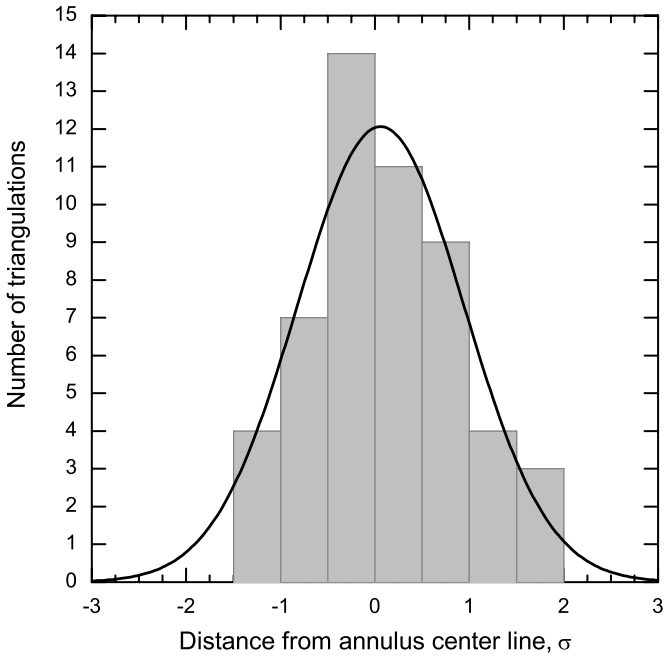

Figure 4. Accuracy of Konus-GBM triangulations. The histogram shows the relative offsets in sigma between the annuli center lines and the XRT counterparts for 52 bursts. The mean is 0.09 and the standard deviation is 0.77. The solid line is a Gaussian fit to the histogram.

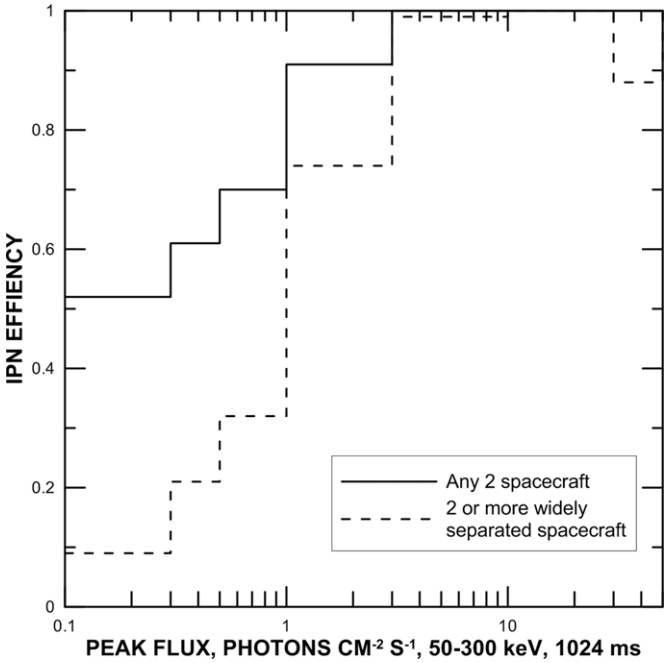

Figure 5. The IPN efficiency as a function of GRB peak flux. The peak flux is measured over a 1024 ms time interval by the GBM in the 50–300 keV energy range. Two efficiencies are shown. The solid line is the probability that any IPN experiment (other than the GBM) will detect the burst. The dashed line is the probability that *Konus*, *Odyssey,* or *MESSENGER* will detect it. Only the latter detections lead to accurate triangulations.

triangulations, because of their larger distances from Earth. From these numbers, we calculate the detection probabilities as functions of flux, fluence, duration, and $E_{\rm peak}$. The results are shown in Figures 5–8. In each of the four graphs, the detection probabilities (or IPN efficiencies) represent an integral over the other three variables, as well as over duty cycles,

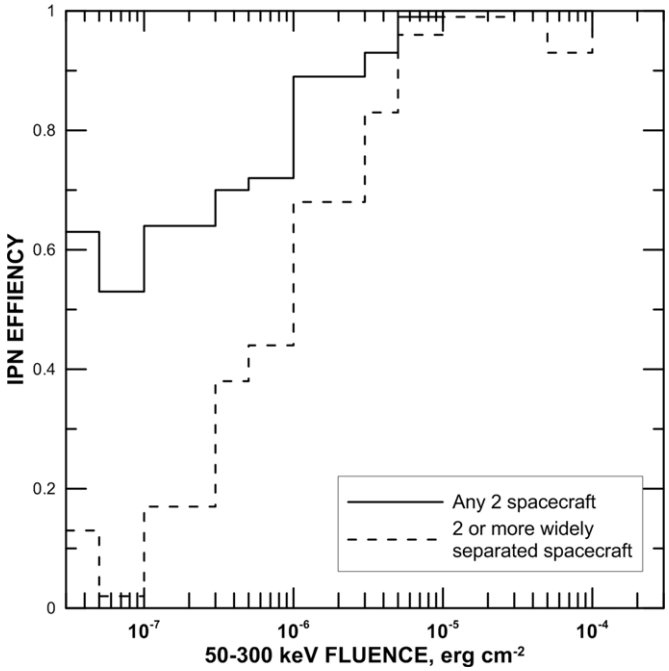

Figure 6. The IPN efficiency as a function of GRB fluence. The fluence is measured by the GBM in the 50–300 keV energy range. Two efficiencies are shown. The solid line is the probability that any IPN experiment (other than the GBM) will detect the burst. The dashed line is the probability that *Konus*, *Odyssey,* or *MESSENGER* will detect it. Only the latter detections lead to accurate triangulations.

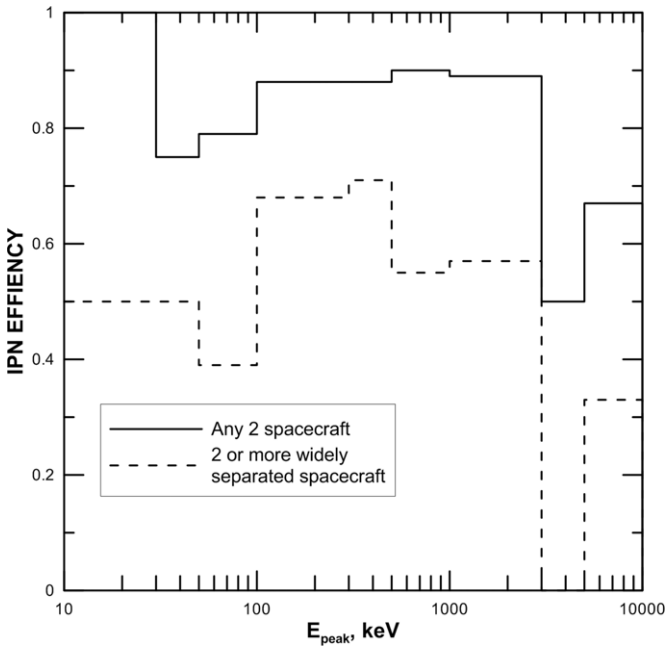

Figure 7. The IPN efficiency as a function of GRB $E_{\rm peak}$. As measured by the GBM, this is from a Band function fit to a single spectrum over the time range of the peak flux of the burst. Two efficiencies are shown. The solid line is the probability that any IPN experiment (other than the GBM) will detect the burst. The dashed line is the probability that *Konus*, *Odyssey,* or *MESSENGER* will detect it. Only the latter detections lead to accurate triangulations. The first and last two bins are based on 12 or fewer events, and have poor statistics.

and, for all the instruments except Konus, planet blocking. The probabilities of IPN detections are 50% or greater for peak fluxes in the range 1–3 photons $\rm cm^{-2}\ s^{-1}$ and for fluences in the range $1–3 \times 10^{-6}$ erg $\rm cm^{-2}$.

Table 2
IPN/GBM Gamma-Ray Bursts

Date	Universal Time[a]	GBM Identifier [b]	Observed by[c]
2008 Jul 14	02:04:12	GRB080714086	Kon
2008 Jul 14	17:52:56	GRB080714745	AGI, INT, Kon, MES, RHE, Swi[e]
2008 Jul 15	22:48:40	GRB080715950	AGI, Kon, MES
2008 Jul 17	13:02:35	GRB080717543	INT
2008 Jul 19	12:41:34	GRB080719529	AGI, INT, Kon
2008 Jul 23	13:22:19	GRB080723557	AGI, INT, Kon, MES[f]
2008 Jul 23	21:56:23	GRB080723913	Suz
2008 Jul 23	23:37:42	GRB080723985	AGI, INT, Kon, MES, Suz
2008 Jul 24	09:37:40	GRB080724401	INT, Kon, RHE, Suz, Swi[d]
2008 Jul 25	10:26:14	GRB080725435	INT, Kon, MES, Swi[e]

Notes.
[a] Universal time is the trigger time of a near-Earth spacecraft.
[b] Two events were not listed as GRBs in the GBM catalog; we have confirmed however that they are valid cosmic events.
[c] AGI: *Astro-rivelatore Gamma a Immagini LEggero* (*AGILE*); INT: *International Gamma-Ray Laboratory*; Kon: *Konus-Wind*; LAT: *Fermi Large Area Telescope*; *MAXI*: *Monitor of All-sky X-ray Image*; MES: *Mercury Surface, Space Environment, Geochemistry, and Ranging* mission; MO: *Mars Odyssey*; RHE: *Ramaty High Energy Solar Spectroscopic Imager*; *RXTE*: *Rossi X-Ray Timing Explorer*; Suz: *Suzaku*; Swi: *Swift*.
[d] Burst was outside the coded field of view of the BAT, and not localized by it.
[e] Burst was localized by *Swift*-BAT; IPN triangulation cannot improve on this localization.
[f] Burst was localized by SuperAGILE and *INTEGRAL*-ISGRI; IPN triangulation cannot improve on this localization.
[g] Burst was localized by *INTEGRAL*-IBIS; IPN triangulation cannot improve on this localization.
[h] Burst was localized by SuperAGILE; IPN triangulation cannot improve on this localization.

(This table is available in its entirety in a machine-readable form in the online journal. A portion is shown here for guidance regarding its form and content.)

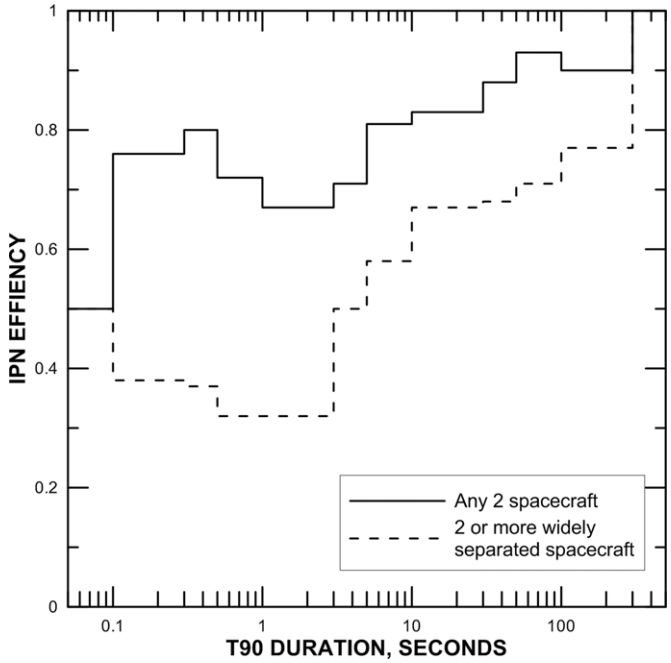

Figure 8. The IPN efficiency as a function of GRB duration. As measured by the GBM, this is T90 in the 50–300 keV energy range. Two efficiencies are shown. The solid line is the probability that any IPN experiment (other than the GBM) will detect the burst. The dashed line is the probability that *Konus*, *Odyssey,* or *MESSENGER* will detect it. Only the latter detections lead to accurate triangulations. The first and last two bins are based on eight or fewer events, and have poor statistics.

Every cosmic burst detected by the GBM was searched for in the IPN data; GBM localizations were used to calculate arrival time windows for *Odyssey* and *MESSENGER*, but the total crossing time windows defined by light-travel times were examined in all cases. The resulting detections are given in Table 2. (Note that this table supersedes the information in Table 2 of Paciesas et al. (2012), which is incomplete.) *Konus* and *Suzaku* can detect bursts in both triggered (2–64 ms time resolution) and an untriggered (1–3 s time resolution) modes; both modes are counted as detections in this table. Also, detections by several instruments which are not part of the IPN have been reported in the table, namely the *Fermi* LAT, *Monitor of All-sky X-ray Image* (*MAXI*), and *Rossi X-Ray Timing Explorer* (*RXTE*).

Two events in Table 2 were detected by the GBM, but did not appear in the GBM catalog. The origin of GRB 091013 was classified as "uncertain." However, the cosmic nature of this event is confirmed by *Konus*. GRB 100501 was detected by numerous IPN spacecraft, including the GBM. However, in that case, the actual GBM trigger was caused by a terrestrial gamma flash.

Whenever *Konus* (in triggered, high time resolution mode), *Odyssey,* or *MESSENGER* detected the burst, we calculated one or more triangulation annuli. The annuli are given in Table 3, and figures may be found in Figure 9. In general, the annuli obtained by triangulations are small circles on the celestial sphere, so their curvature, even across a relatively small GBM error circle, may not be negligible, so that a simple, four-corner error box cannot always be defined accurately. For this reason, we do not cite the intersection points of the annuli with the error circles. A prescription for deriving these points, however, may be found in Hurley et al. (1999a).

When three widely separated experiments observe a burst, the result is two annuli which generally intersect to define two small error boxes. The proximity to the GBM error circle may be used to distinguish the correct one. When *Konus, Odyssey, MESSENGER*, and a near-Earth spacecraft (including *INTEGRAL*) detect a burst, the position is over-determined. In these cases, a goodness-of-fit can be derived for the localization, and an error ellipse can be generated (Hurley et al. 2000a).

Table 3
IPN Annuli

GRB	UT	GBM			IPN								Ecliptic		Planet			Other		
		α	δ	$\sigma_{\rm stat}$	α_1	δ_1	R_1	δR_1	α_2	δ_2	R_2	δR_2	β_1	β_2	α	δ	R	α	δ	R
080715	22:48:40	214.70	9.90	18.97	148.5700	14.4501	60.4476	.2762	273.7129	−26.1484	71.1746	.2884	15.6	35.6	...	...	...	...	...	...
080723	23:37:42	105.30	71.10	18.25	98.9192	24.7391	49.8618	1.5218	158.3648	10.1273	70.8100	.0376	40.0	65.0	...	...	...	...	...	...
080724	09:37:40	358.30	32.90	18.63	99.4409	24.6844	84.6742	.6209	97.4219	21.5770	84.9255	1.1054	35.0	85.0	122.9	−28.4	66.4	...	...	...
080730	12:29:15	245.40	4.60	19.07	284.9798	−23.2105	60.0101	11.7374	...	...	...	...	28.2	48.2	...	...	...	...	...	...
080730	18:51:38	246.60	28.70	19.07	165.8007	6.4610	78.9123	.0519	285.2320	−23.1364	67.9570	.8020	49.3	69.3	...	...	...	...	...	...
080802	09:15:10	154.30	40.70	21.80	105.5186	19.2785	60.6310	1.3190	107.8602	22.3437	56.7793	.2517	4.6	90.0	...	...	...	...	...	...
080803	18:31:20	300.10	82.80	25.24	169.8581	4.3476	84.4750	.4333	110.2713	17.1546	71.7722	11.7110	20.0	90.0	...	...	...	...	...	...
080806	21:29:40	241.80	46.70	19.99	292.5906	−20.8196	79.4133	3.2320	172.9066	2.7178	74.0460	.2645	34.5	90.0	...	...	...	...	...	...
080807	23:50:32	101.70	−16.00	19.62	113.3163	20.6681	32.4763	.3303	...	...	...	...	−36.5	−16.5	...	...	...	...	...	...
080816	12:04:18	156.20	42.60	18.97	181.6313	−2.0874	56.3418	.2924	181.2257	−1.9328	56.0851	.1783	50.0	80.0	...	...	...	...	...	...

(This table is available in its entirety in a machine-readable form in the online journal. A portion is shown here for guidance regarding its form and content.)

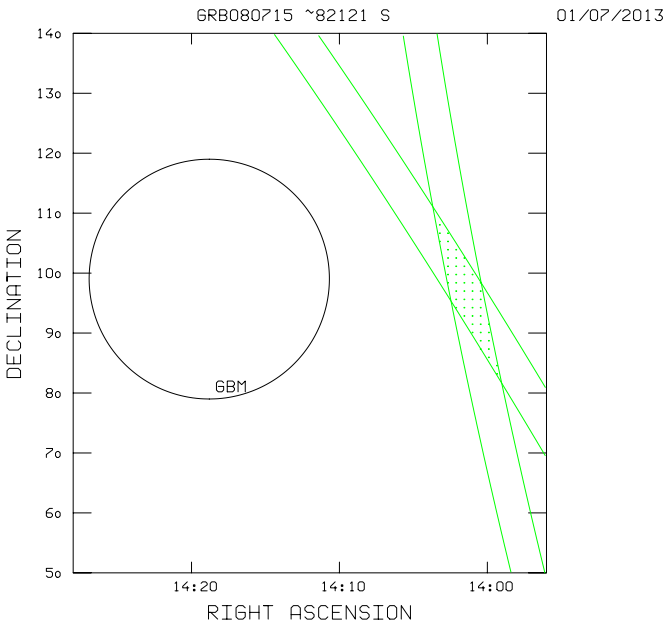

Figure 9. IPN localization of a GBM burst. The following are present in all figures in the figure set. (1) Date in upper right-hand corner: DD/MM/YYYY when the plot was produced. (2) Date and time above the upper right ascension axis: GRBYYMMDD and the approximate time in seconds of day for the burst. This time is actually a fiducial time used for triangulation, and it may differ from the Earth-crossing time by up to minutes in some cases. (3) Right ascension, declination: these are J2000. Not all the figures are to scale; in some cases, changing the aspect ratio displays the IPN error box more clearly. (4) Green lines: annuli obtained by triangulation. These are 3σ confidence regions. (5) Green shading: the region that is common to all the IPN annuli and the ecliptic latitude band (if applicable), but which excludes Earth- and Mars-blocked regions (if applicable). The following are present in some figures in the figure set. (1) Green asterisk: this is used to show the center of an IPN annulus, when the inner radius is zero. (2) Black lines labeled ECLIP.: ecliptic latitude band, from Konus-Wind. These are generally ∼95% confidence regions. (3) Black asterisk: this is used to show the north or south ecliptic pole, when the ecliptic latitude band extends to one of the poles. (4) Earth-N: Earth-blocking, as seen from satellite N. This region is excluded from the localization. (5) Mars: Mars-blocked, as seen from *Mars Odyssey*. This region is excluded from the localization. (6) Circles labeled GBM, LAT, *Swift*, *AGILE*, IBIS: localizations obtained by the *Fermi* GBM, LAT, *Swift*-BAT, SuperAGILE, or *INTEGRAL*-IBIS.

(A color version and the complete figure set (149 images) are available in the online journal)

Although we utilize this procedure whenever possible, we do not quote the localizations as error ellipses in this catalog, because, like the annuli, their curvature can render a simple parameterization inaccurate. A number of degenerate cases can occur in a three-spacecraft triangulation; they are discussed in Hurley et al. (2011b).

When *Konus* and an interplanetary or near-Earth spacecraft observe a burst, it is often possible to define a long, narrow error box from *Konus'* determination of the burst's ecliptic latitude. This is derived from a comparison of the count rates on the two *Konus* detectors, and its accuracy is generally of the order of $\pm 10^\circ$. A study of over 1800 *Konus* events indicates that the ecliptic latitude limits determined in this way can be considered to be an ∼95% confidence band. Systematic uncertainties usually prevent a more accurate determination.

IPN annulus widths are often comparable to, or smaller than, *Fermi* LAT error circle radii, and can therefore reduce the areas of LAT localizations. An example is GRB 090323 (Ohno et al. 2009; Hurley et al. 2009), for which a *Swift* ToO observation led to the discovery of an XRT (Kennea et al. 2009), optical (Updike et al. 2009), and radio (Harrison et al. 2009) counterpart.

3. TABLE OF IPN LOCALIZATIONS

The 21 columns in Table 3 give (1) the date of the burst, in yymmdd format; this contains a link to a figure on the IPN Web site showing the annulus or error box and the GBM error circle, (2) the Universal Time of the burst at Earth, (3) the GBM right ascension of the center of the error circle (J2000), in degrees, (4) the GBM declination of the center of the error circle (J2000), in degrees, (5) the 1σ statistical GBM error circle radius, in degrees, (6) the right ascension of the center of the first IPN annulus, epoch J2000, in the heliocentric frame, in degrees (7) the declination of the center of the first IPN annulus, epoch J2000, in the heliocentric frame, in degrees, (8) the angular radius of the first IPN annulus, in the heliocentric frame, in degrees, (9) the half-width of the first IPN annulus, in degrees; the 3σ confidence annulus is given by $R_{\rm IPN1} \pm \delta\, R_{\rm IPN1}$, (10) the right ascension of the center of the second IPN annulus, epoch J2000, in the heliocentric frame, in degrees, (11) the declination of the center of the second IPN annulus, epoch J2000, in the heliocentric frame, in degrees, (12) the angular radius of the second IPN annulus, in the heliocentric frame, in degrees, (13) the half-width of the second IPN annulus, in degrees; the 3σ confidence annulus is given by $R_{\rm IPN2} \pm \delta R_{\rm IPN2}$, (14) and (15) the Konus ecliptic latitude band, in degrees, (16)–(18) the right ascension, declination, and angular radius of the Earth or Mars, if the planet blocks part of the localization, in degrees, and (19)–(21) any other localization information, in right ascension, declination, and angular radius, in degrees.

The GBM data have been taken from the HEASARC online catalog,[28] if the localization source was "*Fermi*, GBM." For bursts with other localization sources, the "human-in-the-loop" localization was used (V. Connaughton 2012, private communication). GBM localizations are subject to change, and are given here for convenience only. The latest online catalog should be considered to be the most authoritative source of the up-to-date GBM data. The data in Table 3 are also available electronically.[29]

4. A FEW STATISTICS

There are 491 bursts in the GBM catalog (Paciesas et al. 2012). Of these, 427 (87%) were observed by at least one other IPN spacecraft. They are listed in Table 2, and the number of bursts observed by each IPN spacecraft is compiled in Table 4. Those events which were not observed by an IPN spacecraft had fluences between 4.5×10^{-8} and 9.5×10^{-6} erg cm^{-2}, peak fluxes between 0.33 and 8.8 photons cm^{-2} s^{-1}, and durations between 0.13 and 218 s, as measured by the GBM (Goldstein et al. 2012; Paciesas et al. 2012). For 149 of them, it was possible to improve the localizations by triangulation. The minimum and maximum 3σ IPN annulus half-widths were 7.40×10^{-3} and 31.°9, and the average was 1.°8. The IPN error boxes have 3σ areas between about 1 arcmin^2 and 110 deg^2. Each IPN localization was compared to its corresponding GBM error circle, as given in the online catalog.[30] In that catalog, the GBM localizations have been approximated as circles, with 1σ (statistical only) radii. Assuming that they are described by a two-dimensional normal distribution, we would expect 87% of

[28] http://heasarc.gsfc.nasa.gov/cgi-bin/W3Browse/w3query.pl
[29] http://ssl.berkeley.edu/ipn3/index.html
[30] http://heasarc.gsfc.nasa.gov/cgi-bin/W3Browse/w3query.pl

Table 4
Number of GBM Bursts Observed by Each IPN Spacecraft

Konus	*Suzaku*	*INTEGRAL*	*Swift*	*MESSENGER*	*RHESSI*	*AGILE*	*Odyssey*	*MAXI*	*RXTE*
281	199	322	151	126	86	67	56	4	1

the 3σ IPN localizations to agree with them (i.e., to have some intersection with them). We find only 52% agreement.

If a GBM systematic uncertainty of 6° is assumed, and added in quadrature to the statistical uncertainty, we find the expected 87% agreement. If that radius is then multiplied by three, the agreement becomes 98% (3 events with discrepant localizations), so that this can be taken as an approximation to a 3σ GBM confidence region for this particular GRB sample. A more detailed analysis of systematics is given in V. Connaughton et al. (2013, in preparation). Comparing each IPN area with its corresponding 3σ GBM area, as approximated above, we find an average reduction in area of a factor of 180.

5. DISCUSSION AND CONCLUSION

The *Fermi* GBM has proven to be a worthy successor to BATSE. It detects about 245 GRBs yr^{-1} and distributes their coordinates almost instantaneously to a wide astronomical community. The nine-spacecraft IPN is a good complement to it, just as it was to BATSE. It detects a total of about 325 bursts yr^{-1} (18 yr^{-1} are short-duration, hard spectrum GRBs; see Pal'shin et al. 2013), has virtually no planet blocking or duty cycle restrictions when all the spacecraft are considered, and it is capable of good localization accuracy at the cost of longer delays. There are many ground-based experiments, both electromagnetic and non-electromagnetic, which can take advantage of the smaller IPN error boxes, and for which delays are not an issue. In this sense, the GBM and the IPN both expand the reach of *Swift*, by localizing bursts which *Swift* cannot. For example, a search for gravitational radiation is in progress which utilizes the IPN data on over 500 GRBs, the most extensive such search to date; another search has begun for neutrinos, using IceCube data and almost 1000 IPN events.

This catalog represents the first installment of the IPN supplements to the GBM burst catalogs. Work is proceeding on the localization of IPN bursts observed during the third and fourth years of GBM operation. Data on some of these events may be found at the IPN Web site.[31]

Support for the IPN was provided by NASA grants NNX09AU03G (*Fermi*), NNX08AC90G and NNX08AX95G (*INTEGRAL*), NNX08AN23G and NNX09AO97G (*Swift*), NNX08AZ85G and NNX09AV61G (*Suzaku*), NNX07AR71G (*MESSENGER*), and JPL Contracts 1282043 and Y503559 (*Odyssey*). The Konus-Wind experiment is supported by a Russian Space Agency contract and RFBR grant 12-02-00032-a. This research has made use of data and/or software provided by the High Energy Astrophysics Science Archive Research Center (HEASARC), which is a service of the Astrophysics Science Division at NASA/GSFC and the High Energy Astrophysics Division of the Smithsonian Astrophysical Observatory.

REFERENCES

Aptekar, R., Frederiks, D., Golenetskii, S., et al. 1995, SSRv, 71, 265
Del Monte, E., Feroci, M., Pacciani, L., et al. 2008, A&A, 478, L5
Gold, R., Solomon, S., McNutt, R., et al. 2001, P&SS, 49, 1467
Goldstein, A., Burgess, J. M., Preece, R., et al. 2012, ApJS, 199, 19
Harrison, F., Cenko, B., Frail, D., Chandra, P., & Kulkarni, S. 2009, GCN, 9043
Hurley, K., Atteia, J.-L., Barraud, C., et al. 2011a, ApJS, 197, 34
Hurley, K., Briggs, M., Kippen, R. M., et al. 1999a, ApJS, 120, 399
Hurley, K., Briggs, M., Kippen, R. M., et al. 1999b, ApJS, 122, 497
Hurley, K., Briggs, M., Kippen, R. M., et al. 2011b, ApJS, 196, 1
Hurley, K., Goldsten, J., von Kienlin, A., et al. 2009, GCN, 9023
Hurley, K., Guidorzi, C., Frontera, F., et al. 2010, ApJS, 191, 179
Hurley, K., Kouveliotou, C., Cline, T., et al. 2000a, ApJ, 537, 953
Hurley, K., Laros, J., Brandt, S., et al. 2000b, ApJ, 533, 884
Hurley, K., Lund, N., Brandt, S., et al. 2000c, ApJS, 128, 549
Hurley, K., Mitrofanov, I., Kozyrev, A., et al. 2006, ApJS, 164, 124
Hurley, K., Stern, B., Kommers, J., et al. 2005, ApJS, 156, 217
Kennea, J., Evans, P., & Goad, M. 2009, GCN, 9024
Laros, J., Boynton, W., Hurley, K., et al. 1997, ApJS, 110, 157
Laros, J., Hurley, K., Fenimore, E., et al. 1998, ApJS, 118, 391
Marisaldi, M., Labanti, C., Fuschino, F., et al. 2008, A&A, 490, 1151
Meegan, C., Lichti, G., Bhat, P. N., et al. 2009, ApJ, 702, 791
Ohno, M., Cutini, S., McEnergy, J., et al. 2009, GCN, 9021
Paciesas, W., Meegan, C., von Kienlin, A., et al. 2012, ApJS, 199, 18
Pal'shin, V., Hurley, K., Svinkin, D., et al. 2013, ApJS, 207, 38
Rau, A., von Kienlin, A., Hurley, K., & Lichti, G. 2005, A&A, 438, 1175
Smith, D. M., Lin, R., Turin, P., et al. 2002, SoPh, 210, 33
Takahashi, T., Abe, K., Endo, M., et al. 2007, PASJ, 59, 35
Tavani, M., Barbiellini, G., Argan, A., et al. 2009, A&A, 502, 995
Updike, A., Filgas, R., Kruehler, T., Greiner, J., & McBreen, S. 2009, GCN, 9026
Yamaoka, K., Endo, A., Enoto, T., et al. 2009, PASJ, 61, S35

[31] http://ssl.berkeley.edu/ipn3/interpla.html